EARTHQUAKE ENGINEERING AND STRUCTURAL DYNAMICS, VOL. 26, 41–59 (1997)

DYNAMIC INVESTIGATION OF A REPAIRED CABLE-STAYED BRIDGE

C. GENTILE AND F. MARTINEZ Y CABRERA

Department of Structural Engineering, Politecnico di Milano, Piazza Leonardo da Vinci 32, 20133 Milan, Italy

SUMMARY

The theoretical and experimental investigation of a cable-stayed bridge after major repair is described in this paper. Strengthening mainly involved the suspension system (originally with prestressed concrete stays) which was retrofitted by means of external tendons. Full-scale tests were conducted to measure the dynamic response of the repaired system; the experimental program included both traffic-induced and free vibration measurements. A total of 16 vertical frequencies and mode shapes were identified in the frequency range of 0–10 Hz. In the theoretical study, vibration modes involving deck, towers and cables were determined by using finite element models which accounted for the strengthening effects. Two- and three-dimensional models were used so that the importance of three-dimensional modes was estimated as well. The experimental results were compared to natural frequencies and mode shapes computed using theoretical models. For most modes the measured and predicted modal parameters compare well, especially for the vertical modes involving in-phase motion of the stays.

KEY WORDS: ambient vibration; cable-stayed bridges; free vibration; full-scale testing; identification; strengthening

INTRODUCTION

Full-scale testing of real structures is the most reliable way of determining their dynamic properties (e.g. the natural frequencies, mode shapes and damping ratios) and of assessing the validity of theoretical or finite element models. Specifically, dynamic test procedures provide excellent assessment of complex systems such as dams,[1] suspension bridges[2–4] and cable-stayed bridges.[5–7] Furthermore, in recent years full-scale methods were successfully applied to investigate the correlation between structural damage (or repair work) and changes in the modal parameters.[8,9] Numerous discussions on both testing methods and identification procedures can be found, for example, in References 10 and 11.

The results of full-scale testing and computer simulation of a cable-stayed bridge after major repair of the suspension system are described in this paper. The analysed system is part of the Polcevera Creek Viaduct in Genoa, Italy[12,13] which includes three cable-stayed spans and a series of minor spans for a total length of about 1100 m. The cable-stayed systems are characterized by the adoption of prestressed concrete stays, a common feature of bridges designed by R. Morandi in the sixties.[14] A general view of the main spans is shown in Figure 1.

Until a few years ago, it was believed that the concrete cover of the stays was subjected exclusively to the superficial deterioration produced by the unavoidable physical and chemical actions. During the maintenance work of recent years, major damage was detected in the concrete stays of the balanced system no. 11, which is the large span extending to the abutment as indicated in Figure 1. This part of the viaduct will be referred to in the following as BS11.

Once the damage was discovered, a complex intervention of repair[15] was immediately planned and carried out. The strengthening mainly involved: (a) the installation of conventional steel tendons which are flanking the existing concrete stays; (b) the transfer of most tensile force carried by the old suspension system to the external one so that the stiffness supplied by the original cables would be preserved in the repaired structure as well.

CCC 0098–8847/97/010041–19

Received 8 May 1996
Revised 19 July 1996

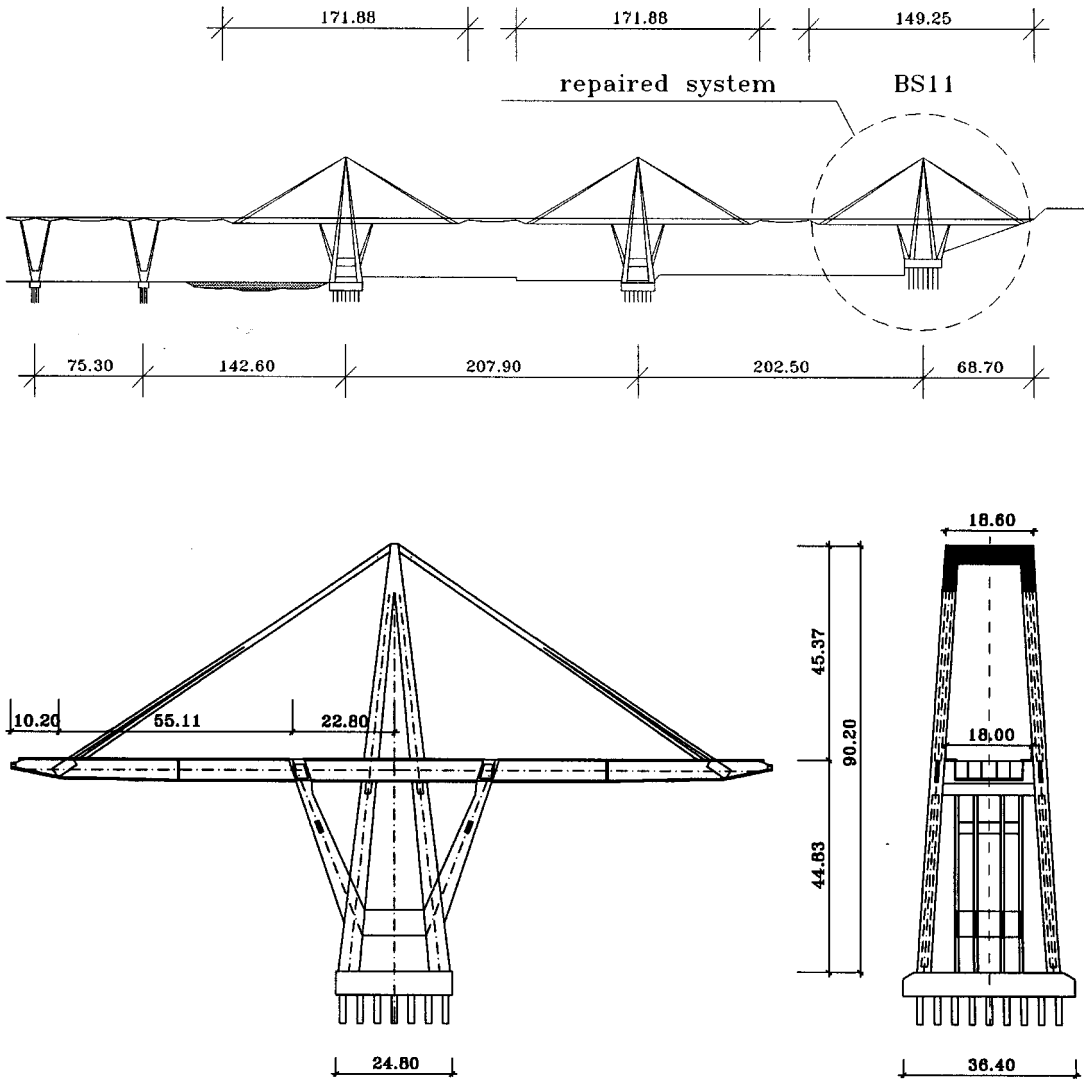

Figure 1. Polvevera Creek Viaduct, general arrangement of the cable-stayed spans (dimensions in metres)

Full-scale dynamic tests (including traffic-induced and free vibration measurements) were conducted over a period of several months while strengthening was in progress in order to trace the changes in the values of modal parameters with the repair;[16] during the tests, the vertical modes were investigated.

The research described in this paper involves:

1. identifying the actual dynamic behaviour from ambient and free vibration responses;
2. assessing the accuracy of ambient vibration survey in view of future monitoring;
3. verifying the assumptions used in formulating two- and three-dimensional models of the repaired bridge through comparison of measured and predicted modal parameters.

DESCRIPTION OF THE STRUCTURE

The Polcevera Creek Viaduct (see Figure 1) was designed by R. Morandi and its construction was completed in 1966. The viaduct, with 11 spans ranging from 43 m to about 208 m, was built in a densely crowded urban area which is occupied by two railroad yards, large industrial plants and the Polcevera Creek.

The three largest spans consist of independent cable-stayed structures, each carried by an individual pier and tower. The suspended spans are connected by simply supported drop-in girders so that the resulting structural scheme is very similar to that used in other well-known bridges (see e.g. Lake Maracaibo[14] or Wadi-Kuf[14]).

In each cable-stayed structure, the roadway deck is a three-span, five-cell box girder (18·00 m wide by 4·50 m deep) with cantilever on each side. The inner supports of the girder are the inclined struts of a V-framed pier while the outer bearings are provided by inclined cables, as shown in Figure 1. The stays are in turn supported by two concrete A-shaped towers which are independent of the pier system supporting the girder, so that any possible damage from differential settlements of piers and towers is prevented.

It should be noted that the BS11 system differs from the others since the backstays and sidespan cantilever extend to the abutment, to which they are anchored through a large concrete block resting on a foundation with inclined piles.

The cable stays of the three main spans consist of pretensioned steel strands encased in a prestressed concrete shell, with a bifurcation in the lower half of the cables. Such unusual elements give the viaduct its unique appearance and have made it famous in the bridge engineering community. The construction of the stays was carried out in successive steps. At the completion of the deck, the stays were made only of conventional 12·5 mm strand tendons which carried the dead load of the cantilever box girder. Successively concrete beams were cast *in situ*, in a segmental way, along the main tendons; the concrete beams were then prestressed by means of additional tendons. Finally, all the tendons were grouted so that the post-tensioned stay-beams (0.92 m wide by 1.32 m deep) supported almost all the live loads.

In the BS11 part of the viaduct, important defects (i.e. local voids dating back to the time of construction) were recently discovered at the anchorage of the stays to the tower; furthermore, non-destructive tests revealed widespread corrosion in the steel wires, which were often locally truncated. This damage demanded a complex intervention of repair which was performed without stopping the traffic, given the importance of the road junction. Full details of the repair procedures are given in Reference 15.

As previously said, the basic idea of the intervention was to transfer the tensile force carried by the existing stay-beams to an external system consisting of conventional steel tendons while keeping nearly unchanged the rigidity of the original suspension system. Thus, the vertical faces of the concrete cables were flanked with $6+6$ primary external tendons, positioned by a series of steel guide collars, as shown in Figures 2 and 3. The new strands were properly anchored to the top of the pylon as well as to the deck overhang or abutment. The load transfer was carried out in successive steps by using a sort of compensation device with $3+3$ secondary tendons which were installed in the lower part of the stays. As an example, the final arrangement of the external tendons at the abutment is shown in Figure 3. It should be noted that the secondary tendons were placed along the two sub-horizontal faces of the existing cables.

Figure 2. General view of the repaired bridge

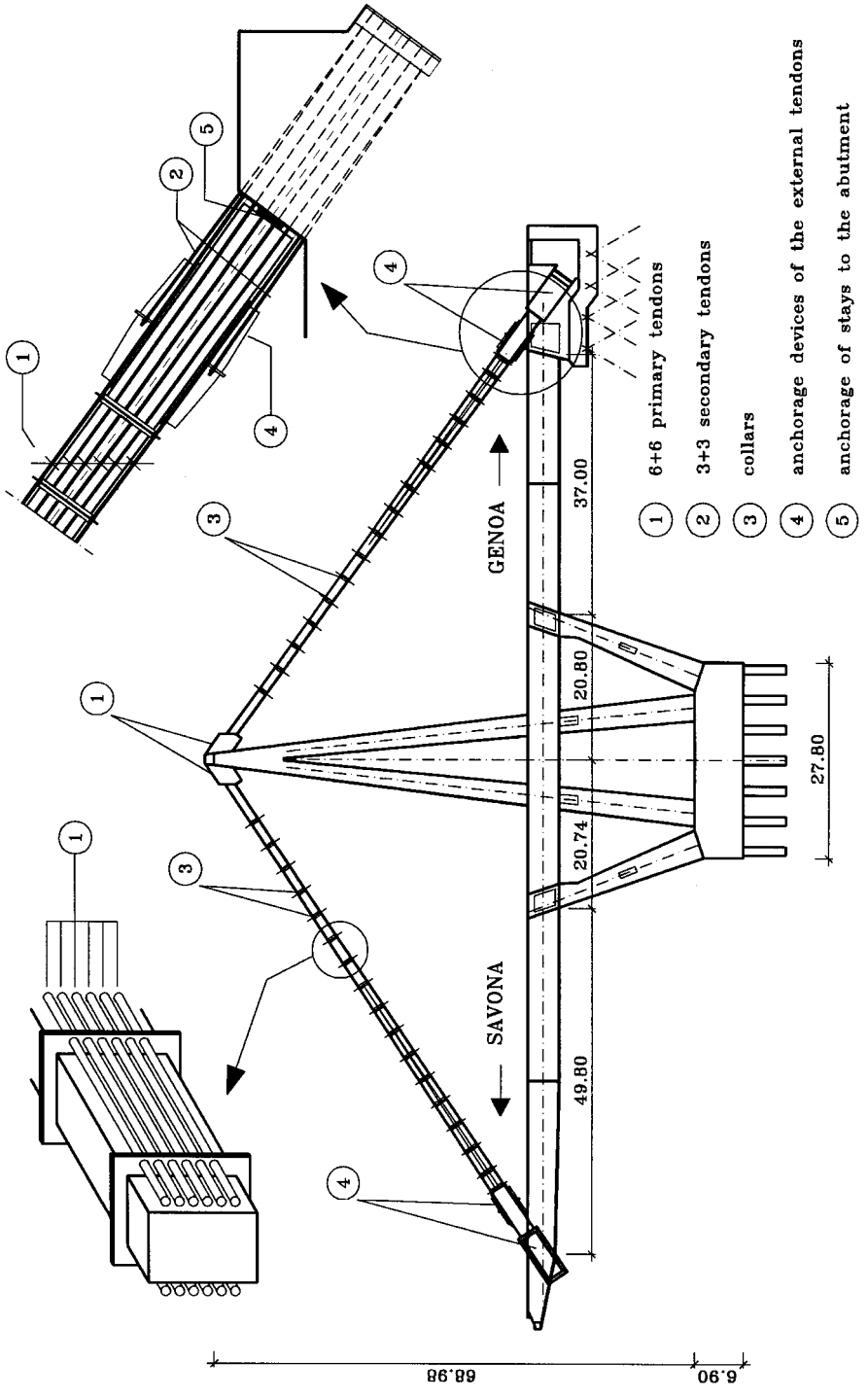

Figure 3. Structural details of the repaired system (dimensions in metres)

It has to be stressed that the load transfer to the external tendons required the terminal portions of the original stays (neighbouring the abutment on the Genoa side and the overhang on the Savona side) to be completely demolished and old wires to be truncated. Thus, in a transitory phase the concrete stays were connected to the deck by the external tendons only. Once the final tension level in the external tendons was reached, the concrete stays were pinned to abutment and overhang through steel devices, as schematically shown in the detail of Figure 3.

FINITE ELEMENT MODELLING AND THEORETICAL DYNAMIC BEHAVIOUR

In the finite element models, only the repaired system was considered. The cable-stayed spans of the viaduct are in fact independent structures which are only connected by simply supported beams.

The linear modelling was based on the assumption that the bridge vibrates around its dead-load state. In the present case, the sag of the cables was known since it was determined by an accurate survey in the field. Furthermore, the tensile forces carried by the original cables and the external tendons were monitored while the repair was in progress. The final tensile forces (used in the numerical analyses) are listed in Table I.

The dynamic behaviour was determined from both a two-dimensional (2-D), vertical plane model and a three-dimensional (3-D) model so that the importance of three-dimensional modes of vibration was estimated. The arrangement of nodal points for the 3-D model (399 nodes, 653 elements) is shown in Figure 4.

Table I. Tensile forces in the suspension system

	T (kN)
Concrete stays, Genoa side	7560
External 3 + 3 secondary tendons, Genoa side	7560
External 6 + 6 primary tendons, Genoa side	17 040
Concrete stays, Savona side	6420
External 3 + 3 secondary tendons, Savona side	6420
External 6 + 6 primary tendons, Savona side	17 040

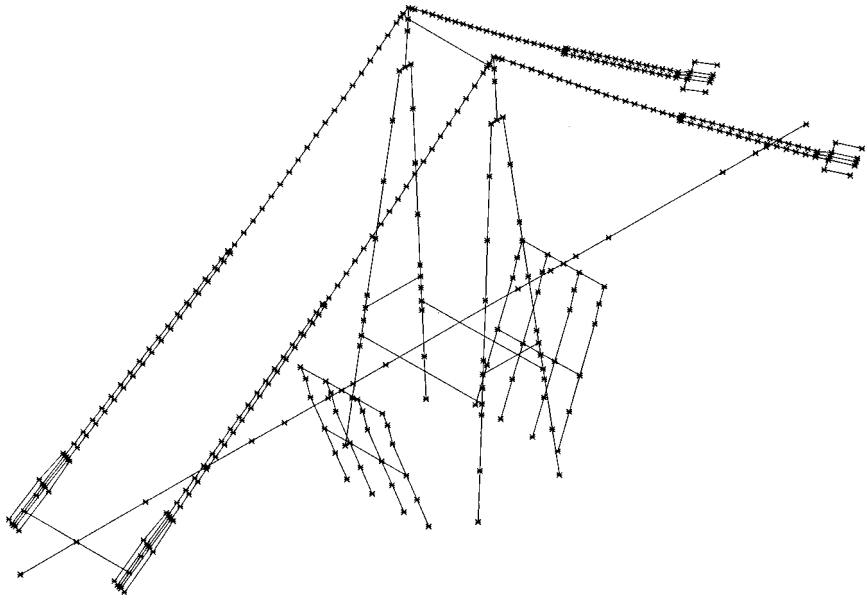

Figure 4. Three-dimensional finite element model of the repaired bridge: nodal points

It should be noted that a regular spacing of nodal points was used to model the stays; the mesh size was determined by the location of both the measurement stations (during the tests) and the steel guide collars.

It is worth underlining that the theoretical models were developed using the following assumptions:

(1) Beam and truss elements were used to represent the concrete stays and the external tendons, respectively.
(2) Steel guide collars were accounted for by means of lumped masses.
(3) No relative displacements were allowed between the concrete cables and the tendons at the collars. This assumption was first suggested by engineering judgement and successively verified from the comparison between theoretical and experimental modal parameters.
(4) The anchorage devices of external primary and secondary tendons were modelled by means of rigid elements.
(5) The connection between existing concrete stay and overhang/abutment was idealized as a simple hinge.
(6) A single spine of beam elements (with a fixed point at the abutment on the Genoa side) was used to model the deck. This simplified representation seems to be satisfactory since the deck consists of a multiple-cell box girder (and hence no significant warping in torsion has to be expected); the stiffness and mass properties in both bending and torsion were evaluated according to classical beam theory.
(7) The large axial forces in concrete cables, external tendons, deck and towers are accounted for by using a geometric stiffness matrix which is added to the elastic stiffness matrix.

Solving the eigenvalue problem of the 3-D model provided the 67 lowest closely spaced modes in the frequency range of 0·656–9·847 Hz. By examining the computed modes of vibration, the following comments can be made:

(a) Most modes may be classified as vertical or lateral. Within the 67 calculated modes, 30 are dominantly vertical (V) and 33 dominantly lateral (L) while strong coupling in the three orthogonal directions (CLV) occurs in a few (4) modes only. This behaviour is conceivably due to the abutment restraint.
(b) A great portion of the bridge dynamic response is associated with motions of the stays since there are 40 pure cable modes (22 being vertical and 18 lateral) and 24 coupled tower–cables (T–C) modes (with or without participation of the deck).
(c) In pure cable modes (showing the usual progression of nodes), each couple of stays vibrates vertically or laterally, either in-phase (C^+) or out-of-phase (C^-). Vertical in-phase motion of the Savona-side stays is usually associated with a vertical vibration of the deck overhang, while out-of-phase modal displacements of the same cables involve deck torsion.
(d) Vertical and torsional vibration of the deck mainly occurs on the Savona side as a consequence both of the abutment restraint and the inclined pier constraint. The dominant lateral motion of the bridge deck is strongly coupled with tower and cables vibration.
(e) The longitudinal motion of the tower is associated with the vertical vibration of deck and cables.

The above-mentioned complicated patterns cannot be represented by two-dimensional modelling which allows a reasonable approximation only for vertical modes with in-phase vibrations of the stays and longitudinal vibrations of the tower.

The characteristics of the three-dimensional modes up to 5 Hz are summarized in Table II. According to the previous comments, the mode shapes can be arranged into the following main types:

1. Modes in which the stays move vertically in-phase (V, C^+) or in-antiphase (V, C^-) with minimal participation of the tower and deck on the Genoa side; (V, C^-) modes are usually associated with torsional vibration of the Savona-side overhang.
2. Modes in which the towers move longitudinally with vertical motion of the cables, either in-phase (V, T–C^+) or in-antiphase (V, T–C^-); (V, T–C^+) modes involve significant deck participation.

Table II. Theoretical vibration modes and natural frequencies of the repaired BS11 system

Mode no.	Mode identifier	Mode shape	Side	Nodes in stays		3-D model f(Hz)	2-D model f(Hz)
				Ge-side	Sv-side		
1	L1	L, C^+	Sv	0	0	0·656	—
2	L2	L, C^-	Sv	0	0	0·720	—
3	V1	V, C^+	Sv	0	0	0·804	0·803
4	L3	L, T—C^+	Ge, Sv	0	1	0·813	—
5	V2	V, C^+	Ge	0	0	0·867	0·885
6	L4	L, T—C^+	Ge, Sv	0	1	0·893	—
7	V3	V, C^-	Ge, Sv	0	0	0·911	—
8	L5	L, C^-	Ge	0	0	0·978	—
9	CLV1	CLV	Ge, Sv	0	1	0·985	—
10	L6	L, T—C^+	Ge, Sv	1	1	1·078	—
11	V4	V, T—C^+	Ge, Sv	0	1	1·535	1·492
12	L7	L, C^-	Sv	0	1	1·849	—
13	L8	L, C^+	Sv	0	1	1·873	—
14	V5	V, C^-	Sv	0	1	1·978	—
15	V6	V, C^+	Ge, Sv	1	1	2·071	2·019
16	V7	V, C^+	Ge	1	0	2·211	2·193
17	V8	V, C^-	Ge	1	0	2·229	—
18	V9	V, T—C^+	Ge, Sv	2	2	2·535	2·755
19	CLV2	CLV	Ge, Sv	2	2	2·573	—
20	L9	L, T—C^+	Ge, Sv	1	2	2·717	—
21	L10	L, C^+	Ge	1	0	2·832	—
22	L11	L, C^-	Ge	1	0	2·859	—
23	L12	L, T—C^+	Ge, Sv	1	2	2·969	—
24	L13	L, C^-	Sv	0	2	2·990	—
25	V10	V, C^-	Sv	0	2	3·152	—
26	V11	V, C^+	Sv	0	2	3·157	3·193
27	L14	L, T—C^+	Ge, Sv	2	3	3·173	—
28	V12	V, C^-	Ge	2	0	3·392	—
29	V13	V, C^+	Ge	2	0	3·462	3·489
30	L15	L, T	—	—	—	3·597	—
31	L16	L, T	—	—	—	4·145	—
32	V14	V, C^+	Ge, Sv	2	3	4·154	—
33	L17	L, C^-	Ge	2	0	4·410	—
34	L18	L, C^+	Ge	2	0	4·419	—
35	V15	V, T—C^-	Ge, Sv	3	3	4·547	—
36	V16	V, T—C^+	Ge, Sv	3	3	4·753	—
37	L19	L, C^-	Sv	0	3	4·817	—
38	L20	L, C^+	Sv	0	3	4·881	—
39	V17	V, C^+	Ge, Sv	3	3	5·025	5·244
40	V18	V, C^-	Ge, Sv	3	3	5·049	—

V = vertical; L = lateral; CLV = coupled lateral—vertical; C^+ = cables in-phase; C^- = cables out-of-phase; T = tower

3. Modes in which the cables move laterally either in-phase (L, C^+) or out-of-phase (L, C^-); (L, C^+) motion is generally coupled with lateral vibration of the deck.
4. Modes in which the towers and the cables move laterally. In-phase cable motion (L, T–C^+) involves lateral vibration of the deck while no significant participation of the deck occurs when the cables move in-antiphase (L, T–C^-).

Representative modes are plotted in Figure 5 which shows plan or elevation or both. Note that the lateral displacements are scaled to zero in the elevation views to enable a better inspection. In both plan and elevation, solid lines indicate the mode shapes and dashed lines the undeformed configuration.

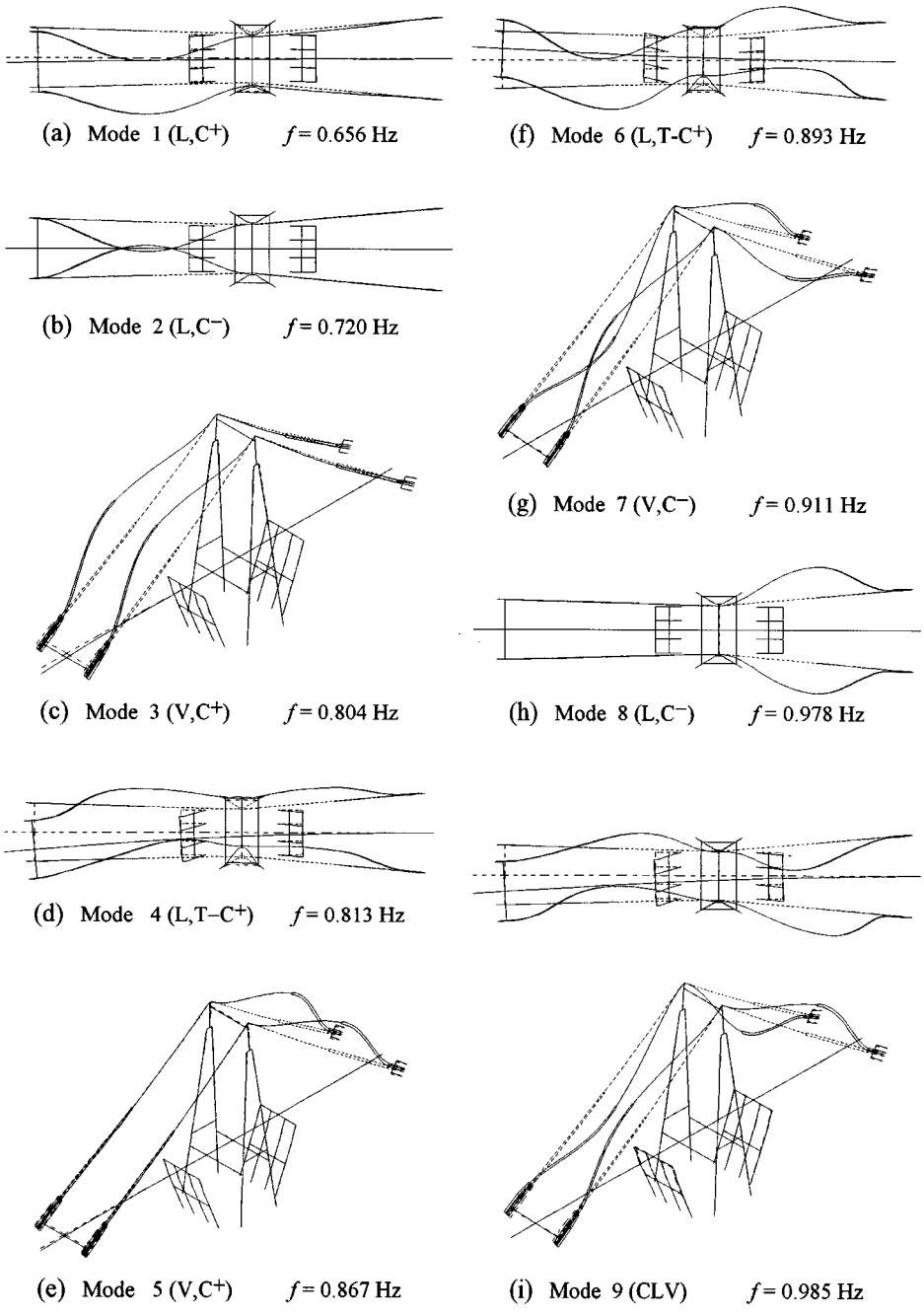

Figure 5. Examples of theoretical modes from 3-D eigensolution

FULL-SCALE DYNAMIC TESTING

The experimental program included both ambient and free vibration measurements; piezometric accelerometers were used to measure the structural response.

Ambient vibration data were recorded for approximately 30 min during each test. The free vibration was easily achieved by the quick release of a pretensioned steel wire, which was connected to one side of the deck

and to the stay on the same side; five different sets of data at least were recorded. During each free vibration test, vehicles were prevented from using the bridge. In order to ease this operation (which was nearly impossible during the day), full-scale testing was completely performed during the night.

Logistics demanded that all measurements were conducted on the southern half of BS11. This seems a satisfactory approach, the system being essentially symmetric about the vertical plane which contains the centreline of the deck girder. The environmental conditions forced to test the two sides (Genoa and Savona) of the bridge separately and to investigate the vertical behaviour.

Detailed measurements were performed in the lower half of each cable-stay because: (a) the strengthening mainly involved the concrete cables; (b) the main structural modifications were placed at the connection between the deck and the stays; (c) finite element analyses indicated that a great amount of the significant dynamic response is associated with the vibration of the stays.

The location of the transducers is summarized in Figure 6. The transducers 5S and 7S measured the vertical motion on the opposite sides (northern and southern half) of the deck overhang. By taking the sum and the difference of the signals, the vertical component of the motion may be separated from the torsional one; these components in turn allow to recognize in-phase and out-of-phase vibration of the stays.

Measurement of the response at the opposite sides of the cross-section was not possible on the Genoa side since a junction slip road is placed on the northern half of the bridge. This seemed not to be a serious loss because no significant torsional motions were to be expected on that side as a consequence both of the abutment restraint and the girder torsional rigidity.

DATA ANALYSIS AND IDENTIFICATION PROCEDURES

Ambient vibration

The extraction of modal parameters from ambient vibration data is based on classical spectral analysis (see e.g. References 17 and 18). Both auto- and cross-spectral estimates are evaluated using the Welch periodogram method;[19] specifically, data were smoothed with a Hanning window and spectra were averaged to give a frequency resolution of 0·025 Hz.

Once the locations of resonant peaks were detected in each autospectrum (provided that the measurement produces nearly unit coherence and near 0 or π phase with all other measurements), natural frequency, damping and amplitude were determined by fitting the power spectral density in the neighbourhood of each peak to the response of a single degree of freedom oscillator. However, this approach is approximate in nature since it requires the normal modes not to interfere significantly and the spectrum of excitation to be nearly flat over the fitted frequency range. Although the latter assumption may not be actually true, similar procedures[4,8] are often used since the error is comparable with that coming from a direct measure of the amplitude and frequency of spectral peaks and an estimate of the damping can be computed with little extra effort as well.

Mode shapes were evaluated by normalizing the amplitudes to the maximum modal value (amplitude 1, phase 0) and cross-spectral phases were used to determine relative phases. Coherence values were computed to assess the quality of data and to investigate the non-linear response of the bridge at each mode.

Typical plots of square root autospectra, cross-spectra and coherence function, which refer to locations from both sides of the bridge, are given in Figures 7–10.

Free vibration

The modal identification from free vibration responses was based on a least-squares output-error procedure in the time domain, which is similar to that used by Beck in Reference 20. Let $\ddot{x}_p^{\mathbf{M}}(t)$ denote the measured acceleration at point p. Using a modal synthesis approach, the calculated output acceleration may be expressed in terms of modal responses $\ddot{q}_k(t)$:

$$\ddot{x}_p(t) = \sum_{k=1}^{N} \phi_{pk} \ddot{q}_k(t) = \sum_{k=1}^{N} \ddot{x}_{pk}(t) \tag{1}$$

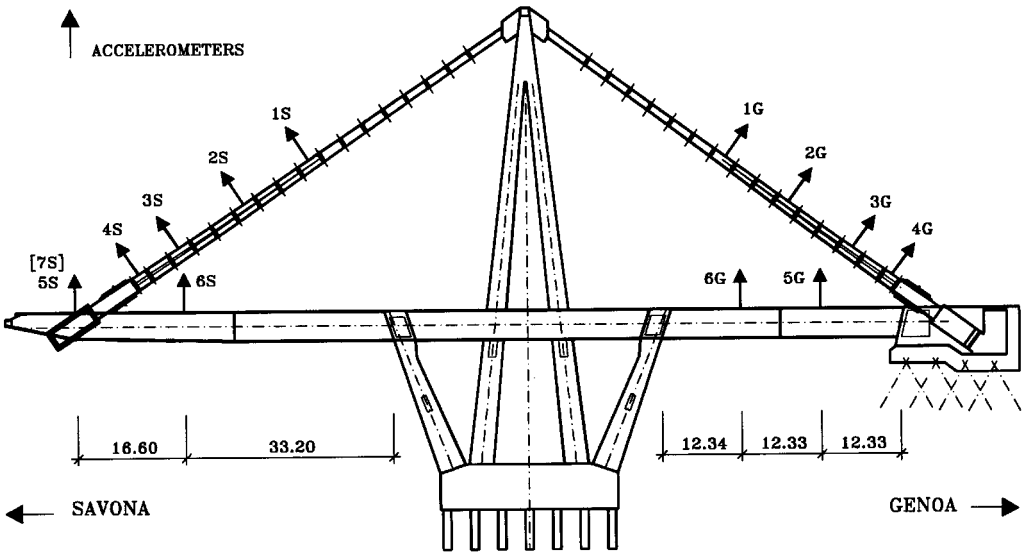

Figure 6. Locations and direction of sensors (dimensions in metres)

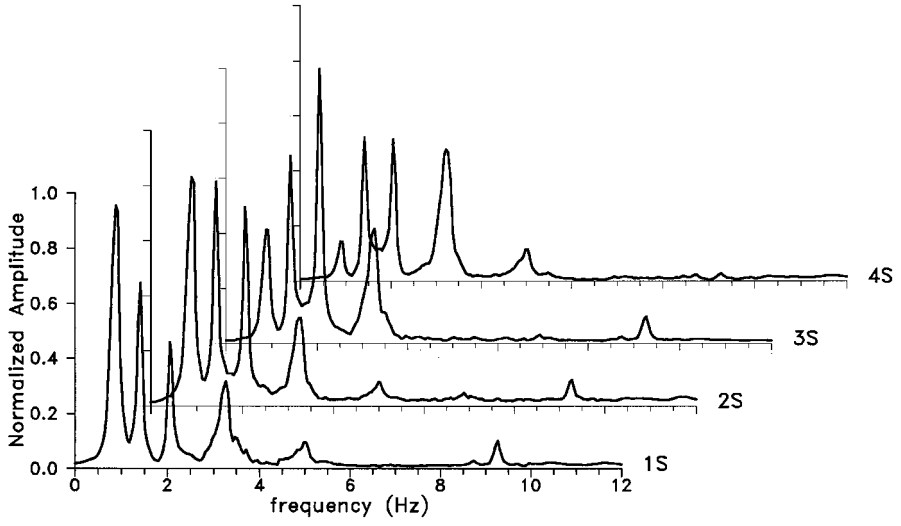

Figure 7. Normalized acceleration spectra from different locations of the Savona-side stay (ambient vibration tests)

where ϕ_{pk} is the mode shape component of the kth mode at location p. Each modal displacement $x_{pk}(t)$ is defined by the second-order differential equation for the classically damped free vibration:

$$\begin{aligned} \ddot{x}_{pk}(t) + 2\zeta_k\omega_k\dot{x}_{pk}(t) + \omega_k^2 x_{pk}(t) &= 0 \\ x_{pk}(t=0) = \phi_{pk}q_k(t=0) &= d_{pk} \\ \dot{x}_{pk}(t=0) = \phi_{pk}\dot{q}_k(t=0) &= v_{pk} \end{aligned} \tag{2}$$

where $\omega_k = 2\pi f_k$ is the undamped frequency, ζ_k is the modal damping ratio and d_{pk}, v_{pk} are the modal contributions to initial displacement and velocity at location p. The acceleration solution of equation (2) only

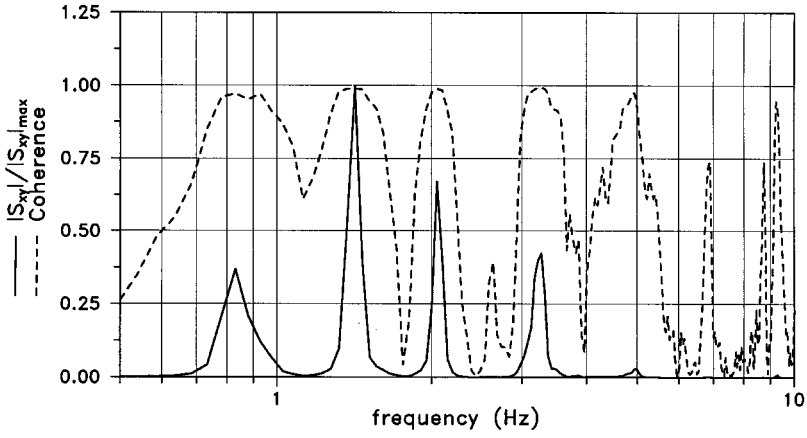

Figure 8. Normalized cross-spectrum magnitude (solid line) and coherence function (dashed line) between measurements at 1S and 4S

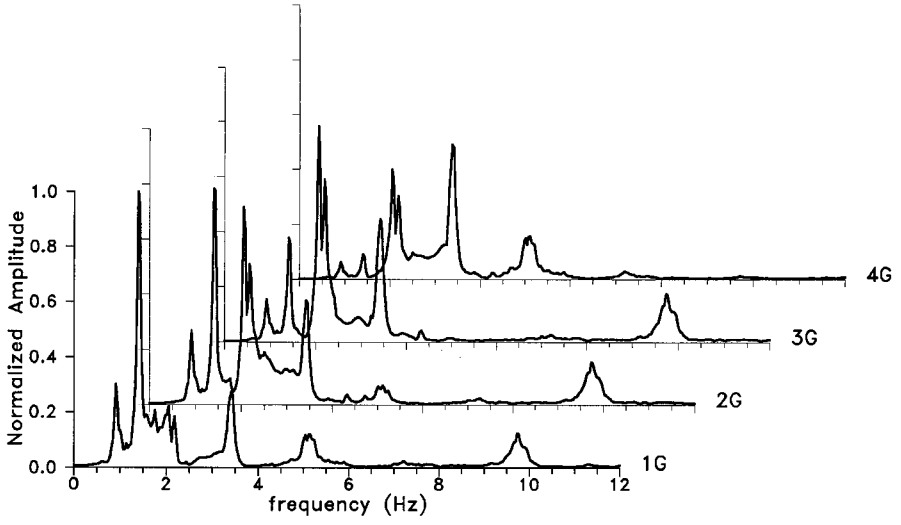

Figure 9. Normalized acceleration spectra from different locations of the Genoa-side stay (ambient vibration tests)

depends on $\mathbf{a}_k = \{f_k, \zeta_k\}^{\mathrm{T}}$, $\mathbf{b}_{pk} = \{d_{pk}, v_{pk}\}^{\mathrm{T}}$ and it can be expressed as follows:

$$\ddot{x}_{pk}(t, \mathbf{a}_k, \mathbf{b}_{pk}) = d_{pk} D_k(t, \mathbf{a}_k) + v_{pk} V_k(t, \mathbf{a}_k) \tag{3a}$$

$$D_k(t, \mathbf{a}_k) = \mathrm{e}^{-\zeta_k \omega_k t} \left(\frac{\zeta_k \omega_k^3}{\omega_{\mathrm{d}k}} \sin \omega_{\mathrm{d}k} t - \omega_k^2 \cos \omega_{\mathrm{d}k} t \right) \tag{3b}$$

$$V_k(t, \mathbf{a}_k) = \mathrm{e}^{-\zeta_k \omega_k t} \left[-\frac{\omega_k^2}{\omega_{\mathrm{d}k}} (1 - 2\zeta_k^2) \sin \omega_{\mathrm{d}k} t + 2\zeta_k \omega_k \cos \omega_{\mathrm{d}k} t \right] \tag{3c}$$

$\omega_{\mathrm{d}k} = \omega_k \sqrt{1 - \zeta_k^2}$ being the damped frequency.

The optimal estimates of the unknown parameters $\mathbf{a}_k, \mathbf{b}_{pk}\,(k = 1, 2, \ldots, N)$ are defined to be the values which minimize the following:

$$J(\mathbf{a}_1, \mathbf{b}_{p1}, \ldots, \mathbf{a}_N, \mathbf{b}_{pN}) = \int_{T_{\mathrm{i}}}^{T_{\mathrm{f}}} \left[\ddot{x}_p^{\mathrm{M}}(t) - \sum_{k=1}^{N} \ddot{x}_{pk}(t, \mathbf{a}_k, \mathbf{b}_{pk}) \right]^2 \mathrm{d}t \tag{4}$$

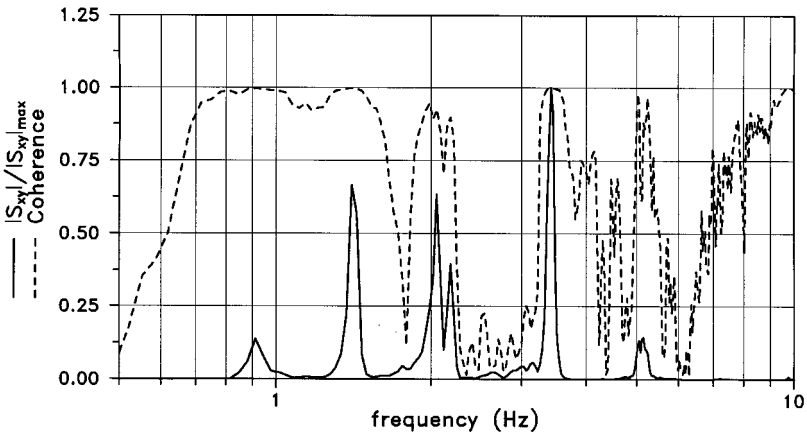

Figure 10. Normalized cross-spectrum magnitude (solid line) and coherence function (dashed line) between measurements at 1G and 4G

The minimization of error criterion (4) is iteratively performed and initial values of natural frequencies and damping ratios (which result from preliminary record analysis using FFT) are only required. In fact, J turns out to depend quadratically on $\mathbf{b}_{pk}$ $(k = 1, 2, \ldots, N)$ since the output acceleration is linear with respect to the same parameters. Thus, for fixed values of $\overline{\mathbf{a}_k}$ $(k = 1, 2, \ldots, N)$ a global minimum of $J(\overline{\mathbf{a}_1}, \mathbf{b}_{p1}, \ldots, \overline{\mathbf{a}_N}, \mathbf{b}_{pN})$ is given by the solution for $\mathbf{b}_{pk}$ $(k = 1, 2, \ldots, N)$ of the linear system of equations which result from setting to zero the partial derivative of $J(\overline{\mathbf{a}_1}, \mathbf{b}_{p1}, \ldots, \overline{\mathbf{a}_N}, \mathbf{b}_{pN})$ with respect to the initial conditions.

The minimization procedure was built to take further advantage of the linearity of equation (3a) and to perform simultaneous optimization with respect to records from different locations in the structure. A brief description of the algorithm is given in the Appendix.

Once the identification phase is completed, the computed time-histories are compared with the actual ones. Typical curve-fits of the measured data are shown in Figure 11(a) and (b), in which the curves refer to the Savona and Genoa sides of the bridge, respectively.

It is worth mentioning that in the quick-release tests the initial velocity v_{pk} $(k = 1, 2, \ldots, N)$ is nearly equal to zero; in practice, this constraint was not applied in the identification procedure but it was used as a further check of accuracy of the results.

DYNAMIC PROPERTIES OF THE BRIDGE

In this section the results of ambient and free vibration testing are presented and compared to the predictions of the previously described model of the repaired bridge. A total number of 16 vertical modes was identified within the frequency range of 0–10 Hz.

Table III summarizes the identified behaviour in terms of natural frequencies, damping ratios, side of the structure (Genoa or Savona) where modal deflections mainly occur and type of the mode. The classification of modes is aimed at evaluating if in-phase ($V1^+$, $V2^+$, ... in Table III) or out-of-phase ($V1^-$, $V2^-$, ... in Table III) motion of the stays occurs. This was easily established for modes involving the Savona side of the bridge from the accelerometers placed at the opposite sides of the cross-section; the modes involving the Genoa side were believed to be associated with in-phase motion of the stays, according to the results of finite element analyses. In this regard, Table III provides the characteristics of the theoretical modes corresponding to the measured ones as well.

Modal parameters from ambient vibration data

The results of ambient vibration testing can be summarized through the spectral plots of Figures 7–10. The normalized acceleration spectra from various locations along the Savona- and Genoa-side stays are shown in

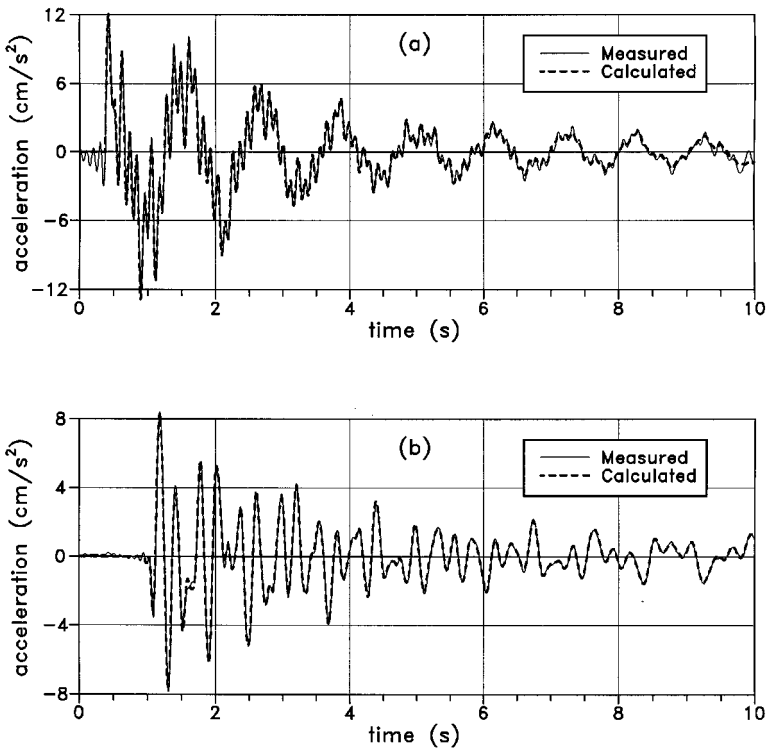

Figure 11. Comparison between measured and calculated free-damped accelerations at: (a) location 2S; (b) location 4G

Table III. Identified modal parameters of the repaired bridge

Experimental modes						Theoretical modes			
		Ambient vibr.		Free vibr.					
Mode identifier	Side	f(Hz)	ς (%)	f(Hz)	ς (%)	Mode shape	Side	3-D f(Hz)	2-D f(Hz)
$V1^+$	Sv	0·841	4·98	0·843	5·63	V, C^+	Sv	0·804	0·803
$V2^+$	Ge	0·908	3·87	0·908	1·06	V, C^+	Ge	0·867	0·885
$V1^-$	Sv	—	—	0·923	1·08	V, C^-	Ge, Sv	0·911	—
$V2^-$	Sv	—	—	1·032	1·07	CLV	Ge, Sv	0·985	—
$V3^+$	Ge, Sv	1·401	2·25	1·421	1·23	V, T—C^+	Ge, Sv	1·535	1·492
$V4^+$	Sv	2·056	1·37	2·054	0·89	V, C^+	Ge, Sv	2·071	2·019
$V5^+$	Ge	2·164	2·25	2·181	0·66	V, C^+	Ge	2·211	2·193
$V3^-$	Sv	—	—	3·162	1·68	V, C^-	Sv	3·152	—
$V6^+$	Sv	3·217	1·99	3·295	1·40	V, C^+	Sv	3·157	3·193
$V7^+$	Ge	3·402	1·39	3·413	1·30	V, C^+	Ge	3·462	3·489
$V4^-$	Sv	—	—	4·167	1·89	V, C^+	Sv	4·154	—
$V5^-$	Sv	—	—	4·716	1·11	V, T—C^-	Ge, Sv	4·753	—
$V8^+$	Ge, Sv	4·982	2·08	5·035	1·36	V, C^+	Ge, Sv	5·025	5·244
$V6^-$	Sv	—	—	6·857	1·32	V, C^-	Ge, Sv	6·893	—
$V9^+$	Sv	9·278	0·90	9·248	0·60	V, C^+	Sv	9·171	9·258
$V10^+$	Ge	9·702	0·82	9·706	0·76	V, C^+	Ge	9·847	9·845

Figures 7 and 9, respectively. These data reveal generally well-defined spectral peaks and a remarkable consistency in their occurrence.

According to theoretical results, experimental mode shapes indicate that most modes involve either the Savona-side cable or the Genoa-side one. Exceptions are represented by the frequencies approximately located at 1·40 ($V3^+$), 2·05 ($V4^+$) and 5·00 ($V8^+$) Hz which are clearly detected on both sides, as shown in Figures 7–10.

Probably as a consequence of the light traffic that existed during the tests, deck torsion was not observed and all the identified modes were related to pure bending vibration of the deck overhang.

The cross-spectrum magnitude (normalized to its maximum value) and coherence function between the measurements at 1S, 4S and 1G, 4G are plotted in Figures 8 and 10, respectively. Note that the coherence is very close to 1 in the frequency range where spectral peaks occur. This information and the consistency of occurrence of modal peaks for different records suggest both a good quality of data and the linearity of the dynamic response. It has to be stressed that the free damped accelerations provided the same conclusion since the identified linear modal models fit very well the measured data (see e.g. Figure 11) and practically the same frequency estimates are obtained using different records and time windows.

Modal parameters from free vibration data

The free vibration testing enables the identification of a greater number of normal modes involving the Savona side of the bridge; nonetheless, Table III shows that free and ambient vibration methods compare very well in terms of natural frequencies (with the maximum differences being less than 1 per cent). A similar match was found in terms of mode shapes (with slightly higher differences) as well; as an example, a global measure of mode shapes correlation like the Modal Assurance Criterion[21] gives a minimum value of 0·987 (for mode $V8^+$).

The agreement of ambient and free vibration results may be stated simply by examining the Fourier amplitudes. As an example, the Fourier spectra of the free-damped acceleration recorded at 1S, 3S and 1G, 3G are given in Figures 12 and 13, respectively. The correspondence is particularly evident for the Genoa side (Figure 13) with the spectral peaks being placed nearly at the same frequencies of Figure 9.

A greater number of peaks is present in Figure 12, which refers to the Savona side and closely spaced frequencies are clearly detected. These close-spaced modes involve either bending or torsion of the deck (and hence in-phase or out-of-phase vertical motion of the stays) as can be verified by computing spectra from the addition and the subtraction of the signals recorded by the two transducers 5S and 7S. The spectral peaks of Figure 14(a) thus correspond to vertical bending modes while torsional modes are shown in Figure 14(b). Again the spectral peaks in Figure 14(a) are located practically at the same frequencies (see Figures 7 and 8) detected in ambient vibration survey.

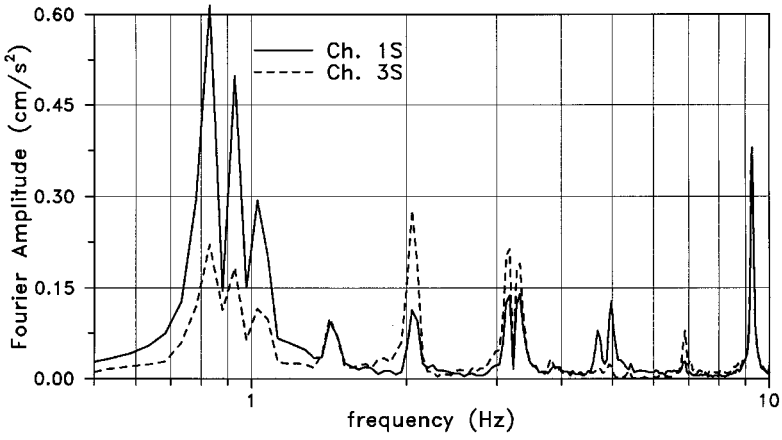

Figure 12. Typical Fourier amplitude from different locations of the Savona-side stay (free vibration tests)

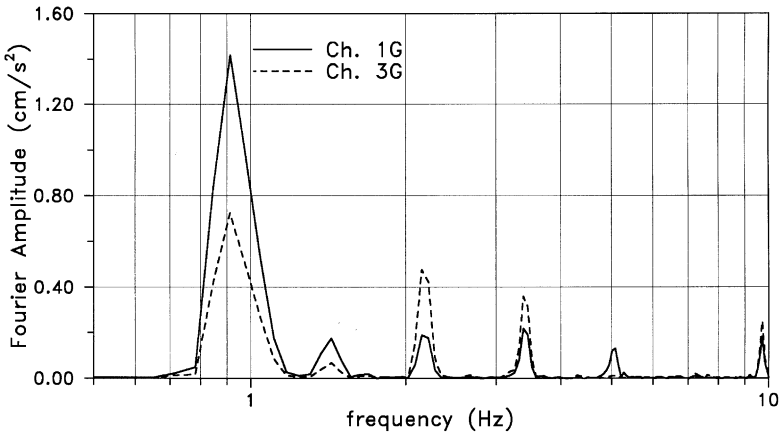

Figure 13. Typical Fourier amplitude from different locations of the Genoa-side stay (free vibration tests)

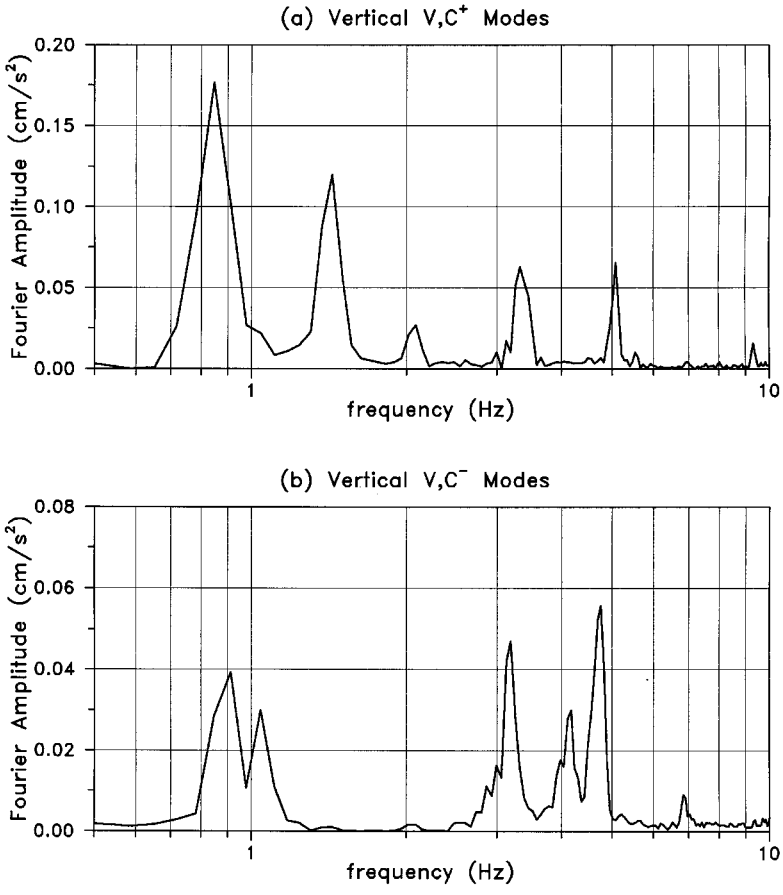

Figure 14. Fourier amplitudes from Savona-side cantilever: (a) vertical (sum of accelerometer signals); (b) torsional (difference of accelerometer signals)

Noticeable differences were detected for the damping ratios, with the ambient estimates being generally much higher than free vibration ones. This fact is consistent with other results reported in the literature (see e.g. References 5 and 8) and is expected since the mass of the bridge–vehicles system is time-dependent; hence, a broadening of response peaks and an increase of the apparent damping may be produced.

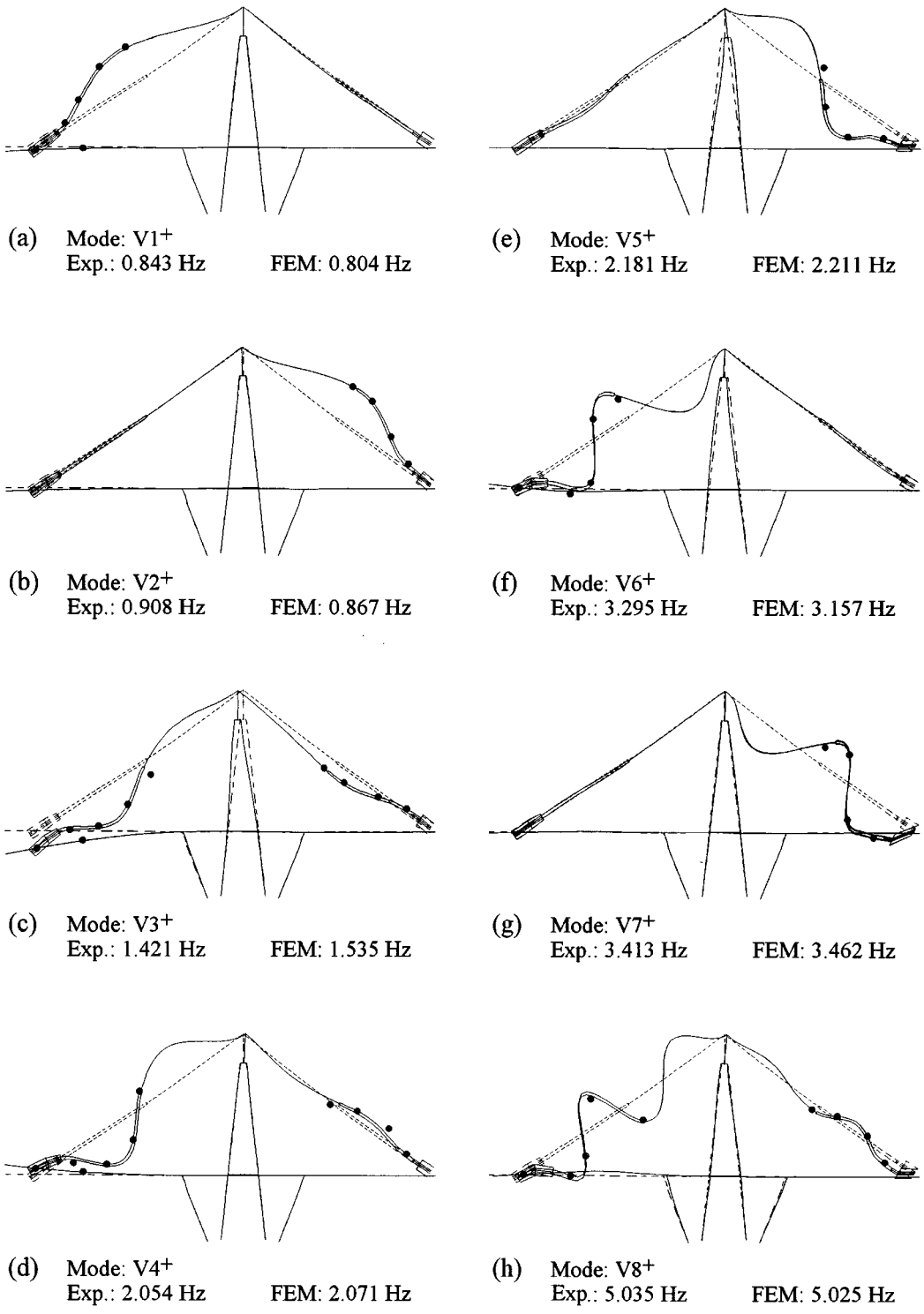

Figure 15. Comparison of theoretical and measured V^+ mode shapes

Since different quick-release tests were performed, the mean values of the natural frequencies and damping ratios are shown in Table III. The variance errors (normalized as $\varepsilon = \sigma/\mu$) turn out to be: (a) very low for natural frequencies ($0.08\% \leqslant \varepsilon_f \leqslant 0.70\%$); (b) low for mode shapes ($0.47\% \leqslant \varepsilon_\phi \leqslant 4.60\%$); (c) rather high for damping ratios ($6.11\% \leqslant \varepsilon_\varsigma \leqslant 11.83\%$).

Comparison with finite element model

As previously said, Table III provides a comparison of experimental and theoretical frequencies obtained from 2-D and 3-D modelling of the bridge. It should be noted that the natural frequencies of the 3-D model are in very close agreement with the actual ones, the maximum difference being 8 per cent for mode $V3^+$ and less than 5 per cent for all the other modes.

In both models, a generally good match is obtained for vertical modes V^+ involving bending deflection of the deck. The measured mode shapes for the above modes are given in Figure 15, where the circles represent measured data points, the solid lines represent the theoretical mode shapes and the dashed lines the configuration of the undeformed system. The computed mode shapes in Figure 15 refer to the 3-D model; thus, modes $V1^+$ and $V2^+$ in Figure 15 (and Table III) correspond to plane representation of modes 3 and 5, respectively, in Figure 5.

The modes V^- can be adequately reproduced by the 3-D model only; again a remarkable correspondence is obtained in terms of natural frequencies and mode shapes (not shown here for brevity) with the exception of the mode $V4^-$; for this mode, the finite element model (see mode 32 in Table II) indicates pure bending of the deck while the measured frequency is clearly associated with deck torsion, as shown in Figure 14(b). This discrepancy is probably due to the simplified modelling of the deck girder.

Furthermore, by examining the measured and computed modal parameters, the following comments can be made:

(a) The mode $V4^+$ ($f = 2{\cdot}054$ Hz) was observed on both sides of the bridge during ambient testing while in free vibration tests it was detected on the Savona side only. This seems fully consistent with the corresponding theoretical mode shape (see Figure 15(d)) which shows higher modal displacements of the Savona-side stays with significant vertical deflection of the overhang; such vertical deflection is very unlikely to be affected by the quick release of a steel wire connected to the opposite-side stay.
(b) The two modes $V1^-$, $V2^-$ (located at 0·923 and 1·023 Hz) were identified only during the free vibration testing of the Savona side while the theoretical mode shapes (shown in Figure 5(g) and 5(i)) indicate a participation of the stays on both sides with torsion of the deck overhang on the Savona side. Again, this torsional motion seems to be very slightly affected by the quick release of a steel wire connected to the Genoa-side stay.

From the above results, it can be concluded that the dynamic behaviour of the repaired bridge is reproduced with good accuracy in the 3-D finite element model. In particular, the simplified coupling of the concrete cables and the external tendons (by neglecting the relative motion at the collars) turns out to be adequate at the low levels of excitation that existed during the tests. Furthermore, the assumptions about the connection of concrete stays and the deck (and in turn the efficiency of such a connection) seem to be verified.

CONCLUSIONS

The full-scale dynamic measurements carried out on the BS11 part of the Polcevera Creek Viaduct have been described. The main interest of the investigation was related with the modifications induced in the suspension system by an important structural retrofit of the stays. Both vehicular excitation and free vibration were employed for full-scale testing. The following main conclusions were drawn from the measurements.

1. Within the frequency range 0–10 Hz, 16 vertical modes were identified. The degree of accuracy of the identified parameters was very good for both frequency and mode shapes while higher scatter was detected for damping values.

2. The results of ambient and free vibration methods compare well in terms of natural frequencies and mode shapes but a greater number of dominant modes was identified during free vibration tests. Specifically, vertical modes with in-phase cable motion and pure bending of deck were detected in both types of test while modes with out-of-phase cable motion and deck torsion were only observed in quick-release tests. This fact was related to moderate traffic conditions that existed during the tests (performed at night). However, the above correspondence suggests the use of ambient vibration survey in future testing of the bridge.
3. Experimental evidence indicated that the small-amplitude dynamic response of the bridge is linear. Ambient vibration data provided in fact consistent coherence and phase information and consistency in the occurrence of spectral peaks for different data records. Free vibration records suggested the same conclusion since an excellent fit of measured data and identified linear modal models was found.
4. The measurements taken in the experimental program were not sufficiently detailed to determine complete mode shapes. However, results of dynamic analysis using a 3-D finite element model of the repaired bridge showed good agreement in both frequencies and mode shapes (at the measurement locations) for vertical modes. This correspondence indicated that the 3-D model is capable of approximately representing the dynamic behaviour of the bridge. Furthermore, the reliability of some fundamental assumptions (i.e. the values of tensile actions in the suspension system, the coupling mechanism of concrete stays and external tendons; the efficiency of the connection of the concrete stays and the deck) seems to be verified.

The comparison of modal parameters before and after repairs[16] allows the further conclusion that the strengthening works mainly cause an increase of modal frequencies (ranging from about 10 to 21 per cent) without significant variations in the relative modal deflections. Although such a feature is usually expected as a consequence of repair, in the present case major uncertainty originated by the modified connection between the stays and the deck.

ACKNOWLEDGEMENTS

The cooperation of G. Camomilla, M. Donferri-Mitelli, F. Rapino and their staff from the Autostrade S.p.a. society is gratefully acknowledged. Furthermore, the authors would like to thank A. Gennari-Santori and the staff from C.N.D. s.r.l society for the valuable assistance in conducting the field tests.

APPENDIX

This appendix provides a description of the algorithm used to minimize the error function (4) with respect to modal parameters $\mathbf{a}_k$, $\mathbf{b}_{pk}$ $(k = 1, 2, \ldots, N)$.

Minimization of J is carried out by a sequence of modal cycles. In each cycle, N single-mode minimizations are performed to get new estimates for the parameters of the N modes of the model. Thus, J is first minimized with respect to the parameters of the first mode $\mathbf{a}_1$, $\mathbf{b}_{p1}$ while keeping the others $\mathbf{a}_k$, $\mathbf{b}_{pk}$ constant. Using the new estimate of $\mathbf{a}_1$, $\mathbf{b}_{p1}$ and the initial values of the other unknowns, minimization of J is then performed with respect to $\mathbf{a}_2$, $\mathbf{b}_{p2}$ and so on.

The linearity of modal acceleration (3a) with respect to $\mathbf{b}_{pk}$ can be exploited to perform iteratively the kth single-mode minimization only with respect to $\mathbf{a}_k$; thus, for the current choice of $\overline{\mathbf{a}_k}$ (and being fixed the others $\overline{\mathbf{a}_i}$, $\overline{\mathbf{b}_{pi}}$ $\forall i \neq k$) the parameters $\mathbf{b}_{pk}$ are computed by solving the linear system of equations:

$$\frac{\partial J(\overline{\mathbf{a}_1}, \overline{\mathbf{b}_{p1}}, \ldots, \overline{\mathbf{a}_k}, \mathbf{b}_{pk}, \ldots, \overline{\mathbf{a}_N}, \overline{\mathbf{b}_{pN}})}{\partial \mathbf{b}_{pk}} = -\mathbf{R}_{pk} + \mathbf{A}_k \mathbf{b}_{pk} = \mathbf{0} \tag{5}$$

being

$$\mathbf{A}_k = \begin{bmatrix} \displaystyle\int_{T_i}^{T_f} D_k^2(t, \overline{\mathbf{a}_k})\, \mathrm{d}t & \displaystyle\int_{T_i}^{T_f} D_k(t, \overline{\mathbf{a}_k}) V_k(t, \overline{\mathbf{a}_k})\, \mathrm{d}t \\ \text{symm.} & \displaystyle\int_{T_i}^{T_f} V_k^2(t, \overline{\mathbf{a}_k})\, \mathrm{d}t \end{bmatrix} \tag{6}$$

$$\mathbf{R}_{pk} = \begin{Bmatrix} \int_{T_i}^{T_f} [\ddot{x}_p^M(t) - \sum_{i \neq k} \ddot{x}_{pi}(t, \overline{\mathbf{a}_i})] D_k(t, \overline{\mathbf{a}_k}) \, dt \\ \int_{T_i}^{T_f} [\ddot{x}_p^M(t) - \sum_{i \neq k} \ddot{x}_{pi}(t, \overline{\mathbf{a}_i})] V_k(t, \overline{\mathbf{a}_k}) \, dt \end{Bmatrix} \tag{7}$$

It should be noted that the matrix $\mathbf{A}_k$ in equation (6) does not depend on the position p but only on the kth modal frequency and damping. This enables the above minimization scheme to handle simultaneous optimization with respect to multiple output records with limited additional amount of computational effort (which is required by the evaluation of $\mathbf{R}_{pk}$ and the solution of a linear system (5) for each measurement station $p = 1, 2, \ldots, r$). In such a case, the error function to be minimized has the following expression:

$$J(\mathbf{a}_1, \mathbf{b}_{11}, \ldots, \mathbf{b}_{1N}, \ldots, \mathbf{a}_N, \mathbf{b}_{r1}, \ldots, \mathbf{b}_{rN}) = \sum_{p=1}^{r} w_p \int_{T_i}^{T_f} \left[\ddot{x}_p^M(t) - \sum_{k=1}^{N} \ddot{x}_{pk}(t, \mathbf{a}_k, \mathbf{b}_{pk}) \right]^2 dt \tag{8}$$

w_p being a weighting constant.

REFERENCES

1. S. T. Mau and S. Wang, 'Arch-dam system identification using vibration test data', *Earthquake eng. struct. dyn.* **18**, 491–505 (1989).
2. V. MacLamore, G. C. Hart and I. R. Stubbs, 'Ambient vibrations of two suspension bridges', *J. struct. div. ASCE* **97**, 2567–2582 (1971).
3. A. M. Abdel-Ghaffar and G. W. Housner, 'Ambient vibration tests of suspension bridge', *J. eng. mech. div. ASCE* **104**, 983–999 (1978).
4. J. M. W. Brownjohn, A. A. Dumanoglu, R. T. Severn and A. Blakeborough, 'Ambient vibration survey of the Bosporus suspension bridge', *Earthquake eng. struct. dyn.* **18**, 263–283 (1989).
5. D. Muria-Vila, R. Gomez and C. King, 'Dynamic structural properties of cable-stayed Tampico bridge', *J. struct. eng. ASCE* **117**, 3396–3416 (1991).
6. J. C. Wilson and T. Liu, 'Ambient vibration measurements on a cable-stayed bridge', *Earthquake eng. struct. dyn.* **20**, 723–747 (1991).
7. J. R. Casas, 'Full-scale dynamic testing of the Alamillo cable-stayed bridge in Sevilla (Spain)', *Earthquake eng. struct. dyn.* **24**, 35–51 (1995).
8. D. F. Mazurek and J. T. DeWolf, 'Experimental study of bridge monitoring technique', *J. struct. eng. ASCE* **116**, 2532–2549 (1990).
9. O. S. Salawu and C. Williams, 'Bridge assessment using forced-vibration testing', *J. struct. eng. ASCE* **121**, 161–173 (1995).
10. G. C. Hart (ed.), *Dynamic response of structures*: *Experimentation*, *Observation*, *Prediction and Control*, ASCE, New York, 1980.
11. D. J. Ewins, *Modal Testing*: *Theory and Practice*, Research Study Press, 1986.
12. R. Morandi, 'The Polcevera Creek viaduct for the Genoa–Savona motorway', *L'industria Italiana del cemento* **37**, 849–872 (1967) (in Italian).
13. R. Morandi, 'Some types of tied bridges in prestressed concrete', *Proc. 1st int. symp. concrete bridge design*, ACI Publication SP-23, 1969, pp. 447–465.
14. M. S. Troitsky, Cable-Stayed Bridges, 2nd edn., BSP Professional Books, 1988.
15. F. Martinez y Cabrera, G. Camomilla, M. Donferri-Mitelli and F. Pisani, 'Rehabilitation of the stays of the Polcevera viaduct', *Proc. int. symp. on cable-stayed bridge*, 1994, pp. 640–665.
16. C. Gentile and F. Martinez y Cabrera, 'Cable-stayed bridge assessment from ambient and free vibration responses', *J. bridge eng. ASCE* (submitted).
17. J. S. Bendat and A. G. Piersol, *Engineering Applications of Correlation and Spectral Analysis*, 2nd edn., Wiley Inmterscience, New York, 1993.
18. D. E. Newland, *Random Vibrations and Spectral Analysis*, Longman Scientific & Technical, 1984.
19. P. D. Welch, 'The use of fast Fourier transform for the estimation of power spectra: a method based on time averaging over short modified periodograms', *IEEE trans. audio electroacoust* **15**, 70–73 (1967).
20. J. L. Beck, 'Determing models of structures from earthquake records', *Report No. EERL 78–01*, California Institute of Technology, Pasadena, California, 1978.
21. R. J. Allemang and D. L. Brown, 'Correlation coefficient for modal vector analysis', *Proc. 1st int. conf. modal anal.*, 1983, pp. 110–116.